

# Solution-Processed Tin Oxide-PEDOT:PSS Interconnecting Layers for Efficient Inverted and Conventional Tandem Polymer Solar Cells

Dario Di Carlo Rasi, Pieter M. J. G. van Thiel, Haijun Bin, Koen H. Hendriks, Gaël H. L. Heintges, Martijn M. Wienk, Tim Becker, Yongfang Li, Thomas Riedl, and René A. J. Janssen\*

Tin oxide nanoparticles are employed as an electron transporting layer in solution-processed polymer solar cells. Tin oxide based devices yield excellent performance and can interchangeably be used in conventional and inverted device configurations. In combination with poly(3,4-ethylenedioxythiophene): polystyrene sulfonate (PEDOT:PSS) as a hole transporting layer, tin oxide forms an effective interconnecting layer (ICL) for tandem solar cells. Conventional and inverted tandem cells with this ICL provide efficiencies up to 10.4% in good agreement with optical-electrical modeling simulations. The critical advantage of tin oxide in an ICL in a conventional tandem structure over the commonly used zinc oxide is that the latter requires the use of a pH-neutral formulation of PEDOT:PSS to fabricate the ICL, limiting the open-circuit voltage ( $V_{OC}$ ) because of its low work function. The  $\text{SnO}_2$ /PEDOT:PSS ICL, on the other hand, provides a nearly loss-free  $V_{OC}$ .

## 1. Introduction

As the global technological development requires an ever increasing amount of energy, it is of fundamental importance to provide ways to exploit renewable sources at a convenient price. Tapping from the most abundant available source of energy, it is of interest to develop low-cost solar energy-converting devices. Although the traditional silicon-based photovoltaic technology is mature and ubiquitous, it does not offer characteristics such as flexibility and semi-transparency, which could likely appeal new shares of the market. To bridge this gap, organic solar cells have been extensively studied in the past two decades. Their technology is based on thin films, which can be conveniently deposited on substrates which are flexible,

stretchable, and bendable.<sup>[1–3]</sup> Moreover, the color of photo-active molecules involved can be chemically tuned almost at will, and the absorber layer made in a semi-transparent fashion.<sup>[4–6]</sup> By

D. Di Carlo Rasi, P. M. J. G. van Thiel, Dr. H. Bin, Dr. K. H. Hendriks, G. H. L. Heintges, Dr. M. M. Wienk, Prof. R. A. J. Janssen  
Molecular Materials and Nanosystems & Institute for Complex Molecular Systems  
Eindhoven University of Technology  
P.O. Box 513, 5600 MB Eindhoven, The Netherlands  
E-mail: r.a.j.janssen@tue.nl

G. H. L. Heintges  
Institute for Materials Research (IMO-IMOMECE)  
Design & Synthesis of Organic Semiconductors (DSOS)  
Hasselt University  
Agoralaan, 3590 Diepenbeek, Belgium


Dr. K. H. Hendriks, Dr. M. M. Wienk, Prof. R. A. J. Janssen  
Dutch Institute for Fundamental Energy Research  
De Zaale 20, 5612 AJ Eindhoven, The Netherlands

T. Becker, Prof. T. Riedl  
Institute of Electronic Devices  
University of Wuppertal  
Rainer-Gruenter-Str. 21, 42119 Wuppertal, Germany

Prof. Y. Li  
Beijing National Laboratory for Molecular Sciences  
CAS Key Laboratory of Organic Solids  
Institute of Chemistry  
Chinese Academy of Sciences  
Beijing 100190, China

© 2019 The Authors. *Solar RRL* Published by WILEY-VCH Verlag GmbH & Co. KGaA, Weinheim. This is an open access article under the terms of the Creative Commons Attribution-NonCommercial License, which permits use, distribution and reproduction in any medium, provided the original work is properly cited and is not used for commercial purposes.

DOI: 10.1002/solr.201800366

 The ORCID identification number(s) for the author(s) of this article can be found under <https://doi.org/10.1002/solr.201800366>.

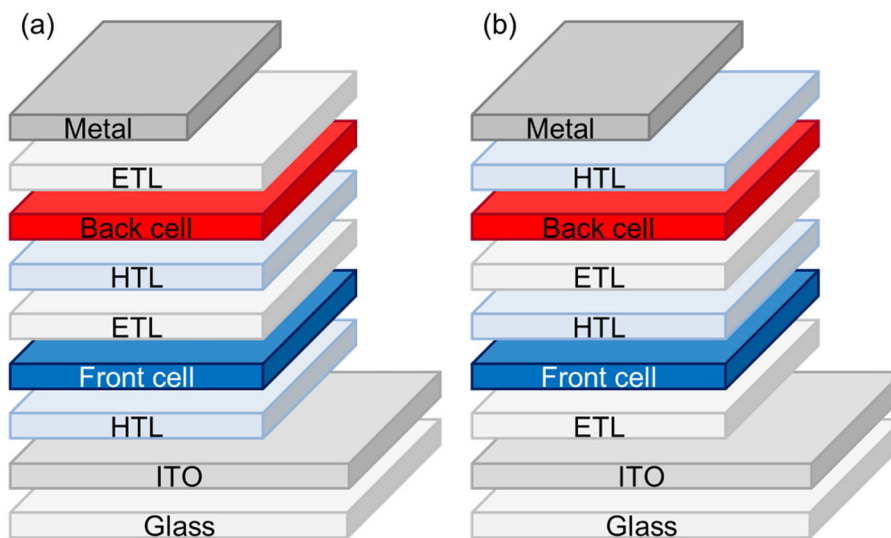


**Figure 1.** Generic stack layouts of conventional (a) and inverted (b) tandem polymer solar cells.

using mixed donor–acceptor bulk-heterojunction layers increasingly higher power conversion efficiencies (PCEs) have been achieved, nowadays above 14%.<sup>[7–10]</sup> Most of the highest efficiency organic solar cells reported up to date are solution-processed devices, in which a blend of an electron-donating polymer and a small molecular electron-accepting species forms the active layer. Such solutions can be conveniently adopted in high-throughput production systems like roll-to-roll or slot-die coating.<sup>[11]</sup> Aiming at further improving the efficiency, solution-processed multi-junction solar cells have been reported,<sup>[12–14]</sup> featuring high efficiencies.<sup>[15,16]</sup> An outstanding 17.3% efficiency has been recently reported for a tandem polymer solar cell entirely processed from solution (apart from the top electrode), thanks to the development of high performing combinations of photoactive materials.<sup>[17]</sup> Depending on the specific arrangement of the electron and hole transport layers (ETL and HTL), we distinguish the conventional and inverted tandem architectures (**Figure 1**). Both configurations use an indium-doped tin oxide (ITO) layer as transparent bottom electrode and a metal layer as reflecting top contact.

The combination of an electron and a hole transporting layer in between the front and back subcells ensures that the two subcells are electrically and optically connected and is referred to as the interconnecting layer (ICL). The sequential deposition from solution of all functional layers represents a challenge to the processing conditions, mainly due to the need for orthogonality of the solvents and sufficient wetting at the same time. A traditional choice for the HTL is poly(3,4-ethylenedioxythiophene):polystyrene sulfonate (PEDOT:PSS), given the good protection it offers against the halogenated solvents from which the photo-active layers are commonly processed.<sup>[18]</sup> As ETL, zinc oxide nanoparticles solubilized in acetone or an alcohol is a widely adopted choice. We recently reported a versatile processing of the ICL for inverted multi-junction polymer solar cells.<sup>[19]</sup> For this, we adopted a combination of PEDOT:PSS in a nearly azeotropic water:1-propanol mixture as HTL and zinc oxide nanoparticles dispersed in isoamyl alcohol as ETL. We

demonstrated several double and triple-junction devices. Unfortunately, the same materials are not suitable to fabricate tandem devices in the conventional configuration. Due to its strong acidity ( $1 < \text{pH} < 2$ ) the PEDOT:PSS dispersion would unavoidably dissolve a previously deposited zinc oxide layer. A workaround consists in replacing the standard acidic formulation of PEDOT:PSS with a pH-neutral one,<sup>[20]</sup> but this is accompanied by a loss in the work function of PEDOT:PSS from 5.05 to 4.65 eV.<sup>[21]</sup> This in turn, results in a non-optimal alignment between the Fermi level of PEDOT:PSS and the HOMO level of the electron-donating polymer in the adjacent active layer, if this is particularly deep. As a consequence, a loss in the open-circuit voltage ( $V_{\text{OC}}$ ) occurs for cells where the polymer has a deeper HOMO and hence the  $V_{\text{OC}}$  is large.<sup>[22]</sup> In practice it is difficult to achieve a  $V_{\text{OC}} > \approx 0.7$  V with pH-neutral PEDOT:PSS,<sup>[23]</sup> but for solar cells with  $V_{\text{OC}} < \approx 0.7$  V ZnO/pH-neutral ICL is virtually without losses.<sup>[24]</sup> The problem for high  $V_{\text{OC}}$  cells can be partly solved. Moet et al.<sup>[22]</sup> proposed the use of Nafion deposited on top of the pH-neutral PEDOT:PSS layer to recover the work function. More recently Lu et al.<sup>[25]</sup> introduced the use of phosphomolybdic acid as surface modifier. Although this approach was successful, it involves an additional functional layer in the ICL, further complicating the fabrication process. Similarly, evaporating an additional layer of  $\text{MoO}_3$  on top of the pH-neutral PEDOT:PSS, before applying the photoactive layer is an option to restore the  $V_{\text{OC}}$ , but also at the cost of an additional, intermediate vacuum processing step.<sup>[26]</sup> Also other commonly used ETLs such as ethoxylated polyethylenimine (PEIE) which can lower the work function of PEDOT:PSS and turn a PEDOT:PSS/PEIE layer into an efficient ICL,<sup>[27]</sup> cannot be used in a conventional ICL configuration in combination with acidic PEDOT:PSS on top, because the PEIE layer is washed away when the aqueous PEDOT:PSS is deposited on top. In fact, relatively few conventional tandem cells have been reported, without using pH-neutral PEDOT:PSS. In early reports on polymer tandem cells,  $\text{TiO}_2/\text{PEDOT:PSS}$  was used as ICL.<sup>[28–30]</sup>  $\text{TiO}_2$ , either as sol-gel or as nanoparticles in the ICL, is more resilient against

acid, but the use of TiO<sub>2</sub> has not received much attention in recent years. Other options are the use of polymer electrolytes. Zhang et al.<sup>[31–33]</sup> used a n-type polymer electrolyte in combination with PEDOT:PSS on the p-side and an ultra-thin silver layer in between to create an ICL. Alternatively, a p-type polymer electrolyte can be placed on top of ZnO nanoparticles to form an ICL.<sup>[34–38]</sup> Che et al.<sup>[39]</sup> used thermally evaporated bathophenanthroline:C<sub>60</sub> (1:1) with an ultrathin Ag nanoparticle layer that allowed processing of acidic PEDOT:PSS on top. Other ICLs involving thermal evaporation are ZnO/Al/MoO<sub>3</sub><sup>[40]</sup> or a hybrid electron transport layer in combination with Al/MoO<sub>3</sub>.<sup>[41]</sup> Ideally, a fully solution-processable ETL with enough chemical stability to withstand the processing of acidic PEDOT:PSS would exist.

Solution-processed tin oxide nanoparticles have emerged as an ETL in the field of perovskite solar cells.<sup>[42]</sup> Also sol-gel tin oxide has been used for organic photovoltaic devices.<sup>[43,44]</sup> Recently, Becker et al.<sup>[45]</sup> presented a tandem polymer solar cell with a molybdenum oxide/tin oxide ICL, where these layers were deposited by thermal evaporation and atomic layer deposition, respectively. Here we demonstrate the use of commercially available tin oxide colloidal dispersions as ETL for the solution-processing of efficient single junction and tandem polymer solar cells with both the inverted and the conventional configuration. For the tandems, tin oxide was used in combination with PEDOT:PSS in the ICL. Two tin oxide formulations were considered in our study, one in water and one in a 1:1 (v/v) mixture of 1- and 2-butanol. In single junction cells the performance of tin oxide as ETL compares well with a perylene

diimide with amino *N*-oxide terminal substituents (PDINO) ETL as reference.<sup>[46]</sup> For the ICL in the inverted tandem configuration a SnO<sub>2</sub> nanoparticles formulation in butanol was used because butanol does not affect a PEDOT:PSS layer. In conventional tandems the tin oxide layer did not dissolve during the deposition of the acidic PEDOT:PSS dispersion. The tandem solar cells with tin oxide afforded efficiencies up to 10.4%, in good agreement with optical-electrical modeling. To further highlight the advantage of solution-processed SnO<sub>2</sub> layers over the ubiquitously used ZnO layers in ICLs of conventional tandem solar cells, we demonstrate that the tandem open-circuit voltage loss for polymers with deep HOMO energy levels can be reduced from 200 to 20 mV when using SnO<sub>2</sub>.

## 2. Results and Discussion

### 2.1. Single Junction Cells With SnO<sub>2</sub> Charge Transport Layers

We fabricated single junction cells in conventional and inverted cell configurations using poly[(4,8-bis(5-(tripropylsilyl)thiophen-2-yl)benzo[1,2-*b*:4,5-*b'*]dithiophene)-*alt*-(5,6-difluoro-2-(2-hexyldecyl)-4,7-di(thiophen-2-yl)-2H-benzo[*d*][1,2,3]triazole)] (J71) blended with 2,2'-[[6,6,12,12-tetrakis(4-hexylphenyl)-6,12-dihydrodithieno[2,3-*d*:2',3'-*d'*]-s-indaceno[1,2-*b*:5,6-*b'*]dithiophene-2,8-diyl]bis[methylydyne(3-oxo-1H-indene-2,1(3H)-diylidene)]]b is [propanedinitrile] (ITIC) (Figure 2).<sup>[47]</sup> For inverted devices we deposited SnO<sub>2</sub> nanoparticles from water (5 wt%) on ITO as ETL

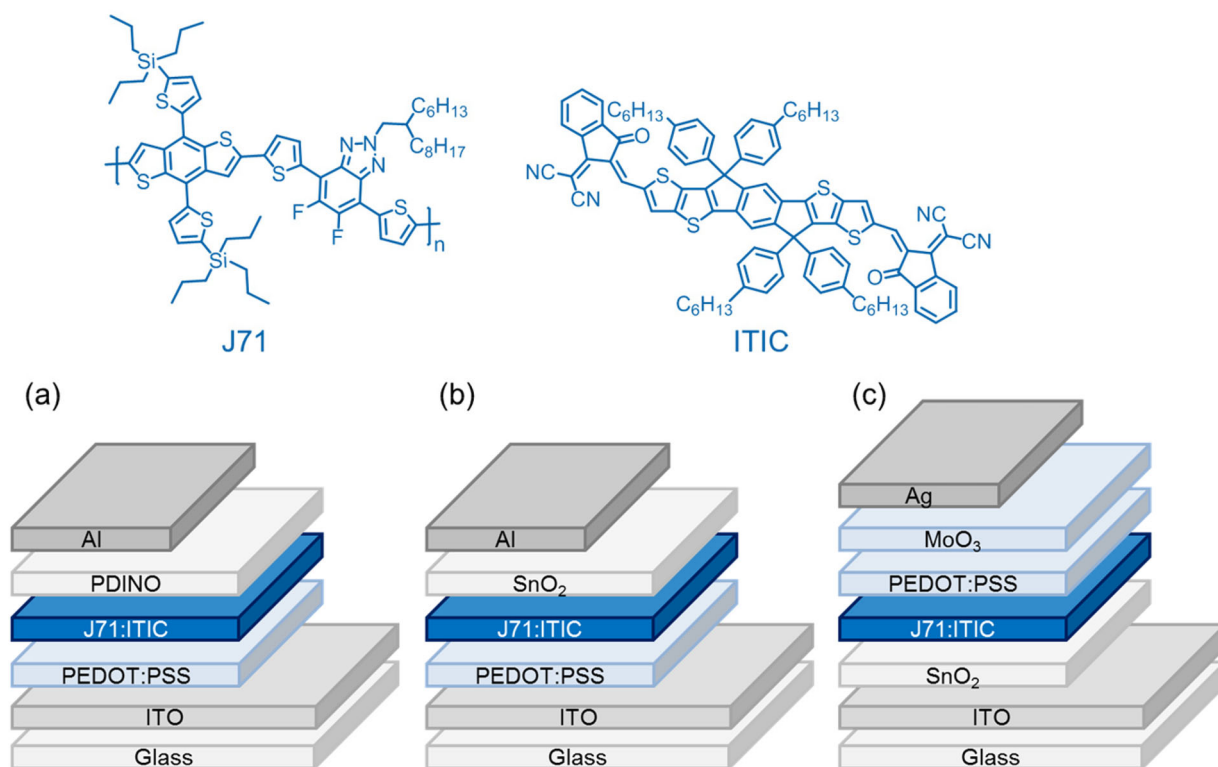


**Figure 2.** Chemical structures of J71 and ITIC. a) Reference device. b) Conventional device. c) Inverted device.

**Table 1.** Photovoltaic parameters of J71:ITIC single junction cells determined with simulated AM1.5G ( $100 \text{ mW cm}^{-2}$ ) illumination.

| Configuration <sup>a)</sup> | $V_{OC}$ <sup>b)</sup> [V] | $J_{SC}^{EQE}$ <sup>c)</sup> [ $\text{mA cm}^{-2}$ ] | FF          | PCE <sup>d)</sup> [%] |
|-----------------------------|----------------------------|--|-------------|-----------------------|
| Reference                   | 0.92 (0.92)                | 15.2 (15.0)  | 0.60 (0.60) | 8.39 (8.28)           |
| Conventional                | 0.93 (0.93)                | 14.8 (14.6)  | 0.58 (0.58) | 7.98 (7.87)           |
| Inverted <sup>e)</sup>      | 0.92 (0.91)                | 15.6 (15.3)  | 0.63 (0.61) | 9.04 (8.50)           |

<sup>a)</sup> Thickness of active layers is 75 nm.

<sup>b)</sup> Values are reported for best cells with average performance over 4 cells in parentheses.

<sup>c)</sup> By integrating the EQE with the AM1.5G spectrum.

<sup>d)</sup> Calculated using  $J_{SC}^{EQE}$ .

<sup>e)</sup> Prior to the measurement, the devices were exposed to UV-light.

(with work function (WF) of 4.0 eV) and PEDOT:PSS as HTL from a water:1-propanol 1:2 (v/v) mixture on the bulk heterojunction layers. For the conventional configuration we used PEDOT:PSS from water on ITO and  $\text{SnO}_2$  nanoparticles from a mixture of 1- and 2-butanol 1:1 (v/v) on the active layer. This  $\text{SnO}_2$  layer served as wetting layer for the subsequent deposition of  $\text{SnO}_2$  nanoparticles in water. Further details are provided in the Experimental Section and Supporting Information. Layers of  $\text{SnO}_2$  nanoparticles have negligible optical absorption in the visible range and show an optical band gap at 3.8–3.9 eV. As a reference, we used a device with PDINO as ETL as published by Bin et al.<sup>[47]</sup> (Figure 2a). The photovoltaic performance of the three devices under simulated air mass 1.5 (AM1.5G,  $100 \text{ mW cm}^{-2}$ ) solar illumination is reported in Table 1 and Figure 3. For 75 nm thick active layer films, the short-circuit current density is fairly close for the three devices ( $14.8 < J_{SC}^{EQE} < 15.6 \text{ mA cm}^{-2}$ ). Compared to the PCE of 11.4% reported by Bin et al.<sup>[47]</sup> the reference device had unfortunately a lower performance because of a lower FF and  $J_{SC}$ . We were unable to identify the origin for the difference in performance, but provide the results to enable a direct comparison with the  $\text{SnO}_2$ -based devices presented in this work. The FF of the conventional cell with  $\text{SnO}_2$  is slightly lower than the reference device (0.58 vs. 0.60, respectively), while it increases for the inverted cell to 0.63. The results in Table 1 demonstrate that solution-processed  $\text{SnO}_2$  layers can be used as effective ETL in single junction polymer cells.

## 2.2. Tandem Solar Cells With $\text{SnO}_2$ and PEDOT:PSS Interconnecting Layer

Prior to making tandem cells in the conventional configuration we tested the integrity of the  $\text{SnO}_2$  layer against the subsequent deposition of an acidic aqueous PEDOT:PSS dispersion. A SEM cross-section image shows a closed  $\text{SnO}_2$  nanoparticle layer after depositing a PEDOT:PSS layer on top from an acidic aqueous dispersion (Figure 4). This demonstrates that the acidic PEDOT:PSS dispersion does not deteriorate the  $\text{SnO}_2$  layer. Kelvin probe experiments showed a WF of 5.0 eV for the ITO/ $\text{SnO}_2$ /PEDOT:PSS stack, close to the WF of 5.1 eV for ITO/PEDOT:PSS.

For the inverted configuration,  $\text{SnO}_2$  from butanol was spin-coated on top of PEDOT:PSS. The WF of an ITO/PEDOT:PSS/ $\text{SnO}_2$  stack determined from Kelvin probe is 4.0 eV, compared to 4.1 eV for a ITO/ $\text{SnO}_2$  layer.

Next, both conventional and inverted tandem devices were fabricated, adopting complementary active layer absorbers for the subcells. J71 blended with ITIC was used as wide band gap front cell absorber, while poly[[2,5-bis(2-hexyldecyl-2,3,5,6-tetrahydro-3,6-dioxopyrrolo[3,4-c]pyrrole-1,4-diyl)-*alt*-[3',3''-dimethyl-2,2':5',2''-terthiophene]-5,5''-diyl] (PMDPP3T)<sup>[24]</sup> in combination with [6,6]-phenyl- $\text{C}_{60}$ -butyric acid methyl ester ( $\text{PC}_{60}\text{BM}$ ) was used as active layer for the small band gap back cell. Figure 5 shows a schematic of the device stack adopted for both configurations and the chemical structures of PMDPP3T and  $\text{PC}_{60}\text{BM}$ . In the conventional configuration, the  $\text{SnO}_2$  layer was deposited in two subsequent steps, first using  $\text{SnO}_2$  nanoparticles in butanol as wetting layer, followed by a layer of  $\text{SnO}_2$  nanoparticles in water. The procedure is detailed in the Supporting Information.

In order to maximize and balance the light absorption in the subcells of the tandem devices, we performed optical simulations using the transfer matrix method on the entire device stacks using the experimentally determined refractive index and extinction coefficients of all layers in the stack. The wavelength-dependent refractive index ( $n(\lambda)$ ) and extinction coefficient ( $k(\lambda)$ ) of the active layers are shown in Figure S1, Supporting Information. These optical simulations were then combined with electrical performance data, acquired from a set of representative single-junction devices of both the subcells, at different thickness of the active layer to obtain

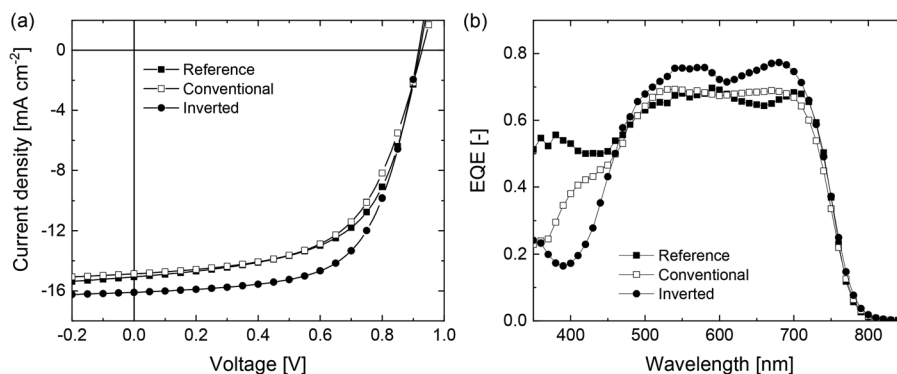


**Figure 3.**  $J$ - $V$  characteristics (a) of optimized reference, conventional, and inverted configuration J71:ITIC single junction cells measured under simulated AM1.5G light ( $100 \text{ mW cm}^{-2}$ ) and corresponding external quantum efficiency spectra (b).



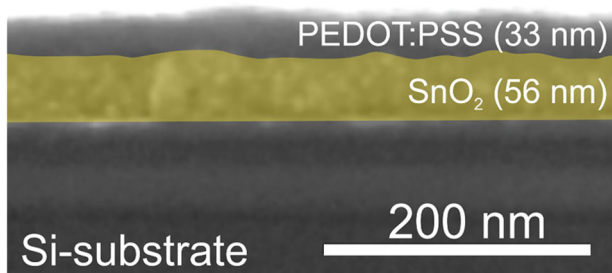


**Figure 4.** Colored SEM cross-section of a PEDOT:PSS layer spin coated on a SnO<sub>2</sub> nanoparticle layer on a Si substrate.

the expected current density–voltage ( $J$ – $V$ ) characteristics of the tandem cells from which the relevant expected device metrics can be determined. The details of this method are described in the literature and in the remainder we refer to it as optical-electrical modeling.<sup>[48]</sup> The precise device structure and photovoltaic parameters of the single-junction cells are reported in Tables S1–S3, Supporting Information. **Figure 6** shows the contour plots of the predicted PCE for the conventional and inverted tandem cells obtained from the optical-electrical modeling.

The highest efficiency predicted for the conventional tandem is 11.1% and corresponds to a thickness combination of 75 nm for the front cell and 125 nm for the back cell. For the inverted tandem the highest PCE expected is 11.7%, and corresponds again to 75 nm for the front cell and 95 nm for the back cell. Because initial experiments on inverted tandem cells gave lower performance than the optical-electrical modeling suggested, we verified experimentally the exact location of the optimum point in the inverted structure. For this we fabricated inverted tandem cells in which the thickness of the front cell was 75 nm, and the thickness of the back cell was increased from 95 to 110 nm and 125 nm and we compared the experimental EQE with the optical-electrical modeling (Figure S2, Supporting Information). While the experimental

EQE of the front cell closely follows the predicted spectral shift with thickness, the experimental EQE of the back cell maximizes at 125 nm, while the optical-electrical modeling suggested 95 nm. For this reason, we chose 125 nm for the thickness of the back cell as the experimental optimum. According to the optical-electrical modeling, this should correspond to a PCE of 10.8%. For the conventional configuration layer stack the PCE of the tandem cell did not improve when changing the thickness compared to the optimum found in the optical-electrical modeling. It is presently not clear what causes the small differences between the modeling and experiments for the inverted tandem cells, but not for the conventional cells. The  $J$ – $V$  characteristics of the optimized tandem cells measured under simulated AM1.5G (100 mWcm<sup>-2</sup>) solar light are shown in **Figure 7** and the relevant parameters are summarized in **Table 2**.

With respect to the optical-electrical modeling, the  $V_{OC}$  is only 2% lower for the conventional structure (1.51 vs. 1.54 V) and 3% lower for the inverted one (1.48 vs. 1.53 V). The fill factor (FF) is in general slightly higher than the modeling: 0.67 vs 0.65 for the conventional cell and 0.63 versus 0.62 for the inverted tandem cell. The experiment and modeling show a higher FF in the conventional tandem cell, than in the inverted tandem cell. This is likely due to the characteristics of the back cell which has a higher FF in the conventional than in the inverted configuration at the 125 nm thickness used (Table S1 and S3, Supporting Information). The experimental and modeled  $J_{SC}$  of the conventional cell deviate by 1 mA cm<sup>-2</sup> (10.10 vs. 11.05 mA cm<sup>-2</sup>). For the inverted tandem the experimental  $J_{SC}$  matches rather well with the optical-electrical modeling (11.10 vs. 11.38 mA cm<sup>-2</sup>). To understand the origin of these deviations and to get in general a better insight, we measured the external quantum efficiency (EQE) spectra of the tandem cells. The EQEs were measured under representative light and voltage bias conditions. The light bias is meant to isolate the response of the individual front and the back cells, while the voltage bias corrects for the electric field induced in the device by the light bias.<sup>[49]</sup> Light emitting diodes (LEDs) centered at 530 and 940 nm were

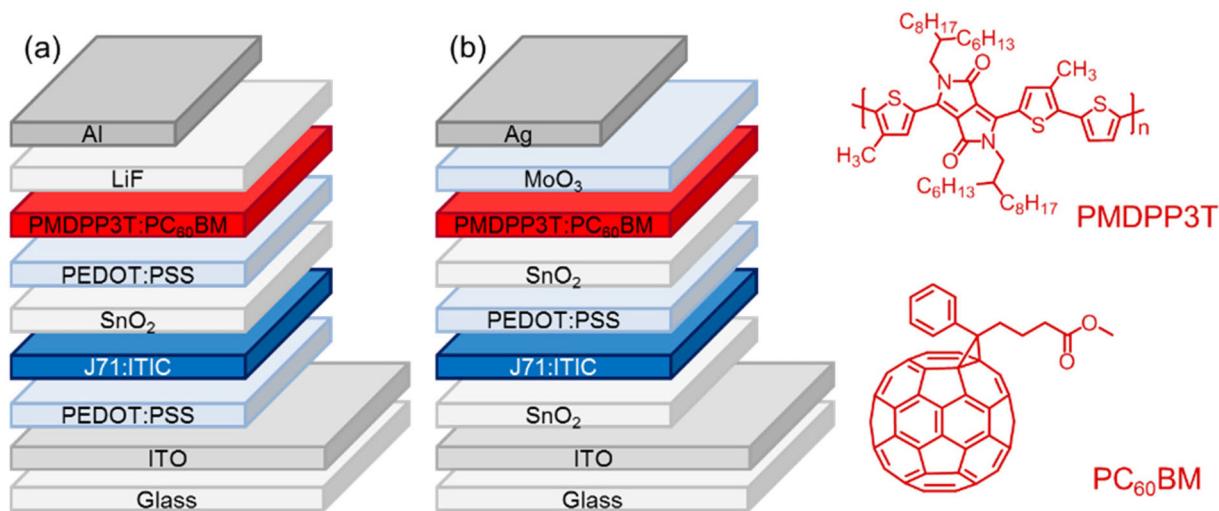


**Figure 5.** Tandem solar cells in the conventional (a) and the inverted (b) configurations and chemical structures of PMDPP3T and PC<sub>60</sub>BM.

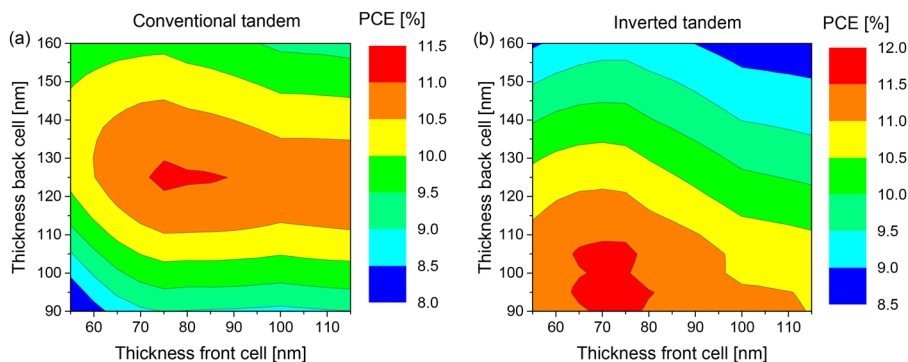


**Figure 6.** Contour plots of the PCE predicted by optical-electrical modeling as a function of the thicknesses of both the front and the back subcells of the conventional (a) and inverted (b) tandem cells.

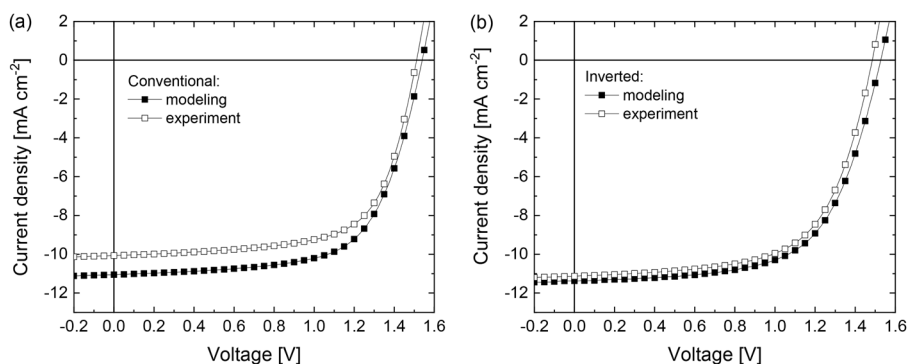


**Figure 7.**  $J$ - $V$  characteristics of optimized conventional (a) and inverted (b) tandem devices measured under simulated AM1.5G light ( $100 \text{ mW cm}^{-2}$ ) (open symbols) and corresponding predicted optical-electrical modeling (solid symbols).

used for optical biasing the front and the back subcells, respectively. The required voltage bias ( $V_{\text{bias}}$ ) was approximated as the  $V_{\text{OC}}$  of the representative single-junction cells, that is,  $V_{\text{bias}} = 0.92 \text{ V}$  for the front cell and  $V_{\text{bias}} = 0.61 \text{ V}$  for the back cell (Table S1 and S2, Supporting Information). Figure S3, Supporting Information, shows the EQE under the different bias conditions. The EQE without light bias follows the lower envelope of the EQE of the subcells, pointing that the contribution of leakage paths is relatively low.<sup>[50]</sup> The effect of

the voltage bias is relatively small, and more significant for the back cell of the inverted tandem. The experimental and optically modeled EQE spectra for both tandem cell configurations are shown in Figure 8. The agreement between optical-electrical modeling and experiment is generally good for both the front and back cells. Minor differences account for the  $1 \text{ mA cm}^{-2}$  drop in the  $J_{\text{SC}}$  for the conventional tandem, with respect to the modeling (Table 2).

**Table 2.** Photovoltaic parameters of tandem solar cells shown in Figure 5 determined with simulated AM1.5G ( $100 \text{ mW cm}^{-2}$ ) illumination.

| Configuration <sup>a)</sup> | $V_{\text{OC}}$ [V] | $J_{\text{SC}}$ [ $\text{mA cm}^{-2}$ ] | FF          | PCE [%]       |
|-----------------------------|---------------------|---|-------------|---------------|
| <b>Conventional</b>         |                     |   |             |               |
| Experiment                  | 1.51 (1.51)         | 10.10 (9.91)                            | 0.67 (0.66) | 10.22 (9.88)  |
| Modeling                    | 1.54                | 11.05                                   | 0.65        | 11.07         |
| <b>Inverted</b>             |                     |   |             |               |
| Experiment                  | 1.48 (1.48)         | 11.10 (10.95)                           | 0.63 (0.63) | 10.35 (10.18) |
| Modeling                    | 1.53                | 11.38                                   | 0.62        | 10.80         |

<sup>a)</sup> Values are reported for best cells with average performance over eight cells in parentheses. All tandems were exposed to UV light prior to the measurement.

### 2.3. Advantage of SnO<sub>2</sub> Over ZnO

The possibility of fabricating a conventional tandem with tin oxide has an important consequence wherever a polymer with a deep-lying HOMO level is used in the back cell to increase the  $V_{\text{OC}}$ . One such example is poly[ $\{2,5\text{-bis}(2\text{-hexyldecyl})\text{-}2,3,5,6\text{-tetrahydro-}3,6\text{-dioxopyrrolo}[3,4\text{-c}]\text{pyrrole-}1,4\text{-diyl}\}\text{-alt-}\{[2,2'\text{-(1,4-phenylene)bisthiophene-}5,5'\text{-diyl}]\}$ ] (PDPPTPT) which has a HOMO energy level of  $5.48 \text{ eV}$ .<sup>[51]</sup> We previously reported that in a conventional tandem cell with zinc oxide and pH-neutral PEDOT:PSS a substantial  $V_{\text{OC}}$  loss occurs because of the mismatch between the HOMO of PDPPTPT and the work function of the pH-neutral PEDOT:PSS.<sup>[23]</sup> In Figure S4 and Table S5, Supporting Information, we show the device characteristics of conventional PDPPTPT:PC<sub>60</sub>BM cells with

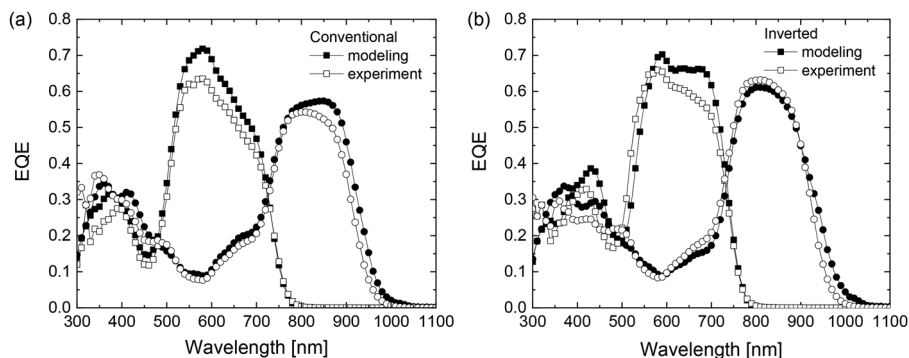


**Figure 8.** Experimental (open symbols) and modeled (solid symbols) EQE spectra of (a) conventional and (b) inverted tandem cells. The EQEs of the front cells are represented with squares while the back cells are reported using circles.

either acidic or pH neutral PEDOT:PSS and find a loss of 100 mV, for the pH neutral PEDOT:PSS HTL. To confirm that this loss does not occur for the new SnO<sub>2</sub>/PEDOT:PSS ICL, we fabricated a PDPPTPT:PC<sub>70</sub>BM homo-tandem cell, that is, using the same active layer for both subcells. Here PC<sub>70</sub>BM is the [6,6]-phenyl-C<sub>71</sub>-butyric acid methyl ester. The device structure was identical to that in Figure 5a, using PDPPTPT:PC<sub>70</sub>BM as active layers. For simplicity, the same layer thickness (100 nm) was used in both subcells. An ITO/PEDOT:PSS/PDPPTPT:PC<sub>70</sub>BM/LiF/Al single junction cell with 100 nm thickness was used as reference. **Table 3** shows the photovoltaic metrics of these devices under simulated AM1.5G solar radiation and **Figure 9** shows the *J*-*V* characteristics.

Having the same active layer in both subcells, the *V*<sub>OC</sub> of the tandem is expected to be twice that of the single junction cell (1.60 V). Experimentally, the tandem cells had a *V*<sub>OC</sub> of 1.54 V, which is 4% lower than expected. Part of this loss is due to the reduced light intensity experienced by the subcells. This loss can be estimated from  $\Delta V_{OC} = (kT/q) \ln[J_{SC}(\text{tandem})/J_{SC}(\text{single})]$ , where *J*<sub>SC</sub>(tandem) and *J*<sub>SC</sub>(single) are the *J*<sub>SC</sub> values of the tandem and the single junction cells (Table 3), and *k* Boltzmann constant, *T* the temperature, and *q* the elementary charge. Since the same absorber is used in both subcells, *J*<sub>SC</sub>(tandem) roughly corresponds to half the *J*<sub>SC</sub>(single) value, as confirmed by the results in Table 3 (7.59 vs. 14.4 mA cm<sup>-2</sup>, respectively). Therefore, we can expect an 18 mV loss at each junction, accounting in total to 36 mV. To confirm this, the reference

single-junction cell was also measured at reduced light intensity, such that it was giving a similar *J*<sub>SC</sub> as the tandem cell. The *V*<sub>OC</sub> measured in this way was 20 mV lower, very close to the predicted loss of 18 mV. The *V*<sub>OC</sub> loss of the tandem which is not directly attributable to the reduced light intensity is then only 20 mV. We note that the additional 20 mV loss is not due to the fact that one subcell in the homo-tandem has SnO<sub>2</sub> as ETL and the reference cell has a LiF/Al contact, because PDPPTPT:PC<sub>60</sub>BM single junction cells with SnO<sub>2</sub>/Al and LiF/Al as contact have the same *V*<sub>OC</sub> (Figure S5 and Table S6, Supporting Information).

To further substantiate the benefit of the SnO<sub>2</sub>/acidic-PEDOT:PSS ICL for conventional tandems, we studied poly[*N*-9'-heptadecanyl-2,7-carbazole-alt-5,5-(4',7'-di-2-thienyl-2',1',3'-benzothiadiazole)] (PCDTBT) in combination with PC<sub>70</sub>BM in single junction and homo-tandem cells. PCDTBT:PC<sub>70</sub>BM single junction cells give a *V*<sub>OC</sub> of 0.90 V and in homo-tandem cell with a SnO<sub>2</sub>/PEDOT:PSS ICL 1.73 V (Figure S6 and

**Table 3.** Photovoltaic parameters of single and homo-tandem cells based on PDPPTPT:PC<sub>70</sub>BM in a conventional structure determined with simulated AM1.5G (100 mW cm<sup>-2</sup>) illumination.

| Configuration <sup>a)</sup>   | <i>V</i> <sub>OC</sub> [V] | <i>J</i> <sub>SC</sub> [mA cm <sup>-2</sup> ] | FF          | PCE [%]     |
|-------------------------------|----------------------------|---|-------------|-------------|
| Single junction               | 0.80 (0.79)                | 14.4 (14.4)                                   | 0.63 (0.62) | 7.23 (7.03) |
| Single junction <sup>b)</sup> | 0.78 (0.78)                | 7.34 (7.37)                                   | 0.66 (0.65) | 3.77 (3.72) |
| Tandem                        | 1.54 (1.54)                | 7.59 (7.48)                                   | 0.58 (0.58) | 6.82 (6.69) |

<sup>a)</sup> See the main text for a description. Values are reported for best cells with average performance in parentheses. The statistics is over four identical cells for the single junction devices and 8 cells for tandems.

<sup>b)</sup> These measurements were performed under reduced light intensity to mimic the behavior of the subcells in the tandem.

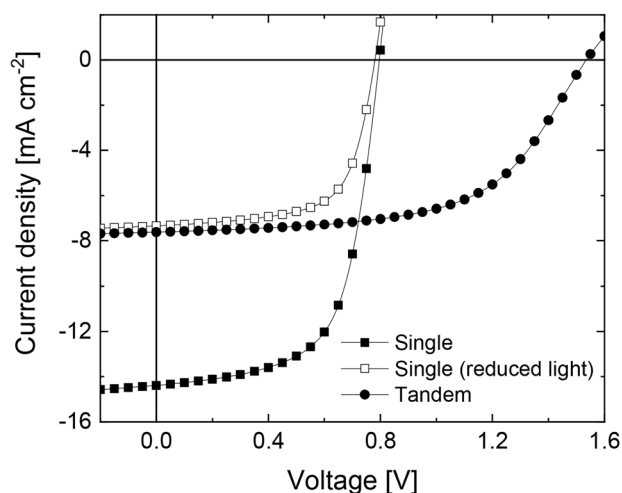


**Figure 9.** *J*-*V* characteristics of single and homo-tandem cells based on PDPPTPT:PC<sub>70</sub>BM in a conventional structure determined with simulated AM1.5G (100 mW cm<sup>-2</sup>) illumination. The single junction cell has also been measured with reduced light intensity to mimic the behavior of the subcells in the tandem.

Table S7, Supporting Information). This implies a 70 mV loss, similar to the 60 mV loss found for the PDPPTT:PC<sub>70</sub>BM cells.

These results are significantly better than what was reported earlier for similar tandems using zinc oxide and pH-neutral PEDOT:PSS, where the  $V_{OC}$  loss was much larger.<sup>[23,26]</sup> This confirms that a SnO<sub>2</sub>/acidic-PEDOT:PSS ICL gives superior performance compared to a ZnO/pH-neutral-PEDOT:PSS ICL for polymers with deep HOMO levels.

### 3. Conclusions

Commercially available tin oxide nanoparticles dispersions in water or butanol are adopted in the fabrication of polymer solar cells. Both conventional (*p-i-n*) and inverted (*n-i-p*) solar cells can be built using tin oxide as ETL and PEDOT:PSS as HTL in the interconnection layer. The two materials are not only chemically compatible with each other, but they also provide an effective interconnection of the subcells, as demonstrated by two high efficiency tandems with PCEs of 10.2% (conventional) and 10.4% (inverted), in good agreement with the performance predicted by optical-electrical modeling. The use of SnO<sub>2</sub> and its resilience against acidic aqueous PEDOT:PSS dispersions has an important advantage compared to the commonly used ZnO/pH-neutral PEDOT:PSS ICL, when donor materials with deep-lying HOMO energy level are involved, because the voltage losses associated with the use of pH-neutral PEDOT:PSS<sup>[23,26]</sup> are eliminated. In conclusion, SnO<sub>2</sub> and PEDOT:PSS can be used as ICL for efficient conventional and inverted tandem cells, without the need of additional layers to reach optimal performance. Together, these results pave the way to new possibilities in the framework of manufacturing efficient multi-junction organic solar cells.

### 4. Experimental Section

**Materials:** Pre-patterned ITO (190 nm) on glass substrates were purchased from Naranjo Substrates. Molybdenum trioxide powder (99.97%) was purchased from Sigma-Aldrich. The tin oxide layers were made by spin-coating a suspension of pre-formed nanoparticles. These were either tin oxide in water (15 wt%, Alfa Aesar) or in a mixture of 1- and 2-butanol 1:1 (v/v) (N31, 2.5 wt%, Avantama). The concentration of the aqueous dispersion was adapted by diluting the stock dispersion with water. The SnO<sub>2</sub> dispersion in butanols was used as received. The suspension of PEDOT:PSS (Clevios P VP Al 4083, Heraeus) was filtered with a 0.45 μm PVDF filter and directly used or diluted with 1-propanol while vigorously stirring (referred to as D-PEDOT:PSS).<sup>[19]</sup> A dilution ratio of 1:2 (v/v) was used by adding n-propanol (1 mL) to PEDOT:PSS (Clevios P VP Al 4083, 0.5 mL) in 15 min under constant vigorous stirring. The suspension was prepared right before depositing D-PEDOT:PSS, and no further additives were used. pH-neutral PEDOT:PSS (PEDOT-NT5, batch number 3435695/2, Agfa) was used as received. ZnO layers were made via a sol-gel route, starting from a solution 0.5 M Zn(CH<sub>3</sub>COO)<sub>2</sub> · 2H<sub>2</sub>O (98%, Acros Organics) and 0.5 M ethanalamine in 2-methoxyethanol.<sup>[52]</sup> PDINO was synthesized according to the procedure reported in literature and dissolved in methanol with a concentration of 1 mg mL<sup>-1</sup>.<sup>[46]</sup> PC<sub>60</sub>BM and PC<sub>70</sub>BM were purchased from Solenne while ITIC was purchased from Solarmer. Poly[(4,8-bis(5-(tripropylsilyl)thiophen-2-yl)benzo[1,2-*b*:4,5-*b'*]dithiophene)-*alt*-(5,6-difluoro-2-(2-hexyldecyl)-4,7-di(thiophen-2-yl)-2H-benzo[*d*][1,2,3]triazole)] (J71) was synthesized according to the procedure reported in literature and blended with ITIC with a 1:1 weight ratio.<sup>[47]</sup> The two components were dissolved in chloroform at a concentration of

6 mg mL<sup>-1</sup> of polymer. Poly[[2,5-bis(2-hexyldecyl-2,3,5,6-tetrahydro-3,6-dioxopyrrolo[3,4-*c*]pyrrole-1,4-diyl)-*alt*-(3',3''-dimethyl-2,2':5',2''-terthiophene)-5,5''-diyl] (PMDPP3T) was synthesized following the reported procedure.<sup>[24]</sup> PMDPP3T was blended with PC<sub>60</sub>BM (1:3 weight ratio) and dissolved in a solution of chloroform, containing 7 vol.% *o*-dichlorobenzene. The concentration of polymer was 3 mg mL<sup>-1</sup>. Poly[[2,5-bis(2-hexyldecyl)-2,3,5,6-tetrahydro-3,6-dioxopyrrolo[3,4-*c*]pyrrole-1,4-diyl)-*alt*-[[2,2'-(1,4-phenylene)bisthiophene]-5,5'-diyl]] (PDPPTT) was synthesized according to the procedure reported in literature.<sup>[51]</sup> This polymer was blended with PC<sub>70</sub>BM 1:2 (w/w) in chloroform with 6 vol.% *o*-dichlorobenzene at a polymer concentration of 5 mg mL<sup>-1</sup>. PCDTBT polymer (1-Material) was blended in a 1:4 ratio with PC<sub>70</sub>BM and dissolved in chlorobenzene at a PCDTBT concentration of 7 mg mL<sup>-1</sup>.

**Device Fabrication:** The patterned ITO substrates were cleaned by sonication in acetone, followed by a solution of sodium dodecyl sulfate in water. They were then rinsed in water and sonicated in isopropanol, before being treated under a UV/Ozone lamp to complete the cleaning. Molybdenum oxide (10 nm), silver (100 nm), lithium fluoride (1 nm), and aluminum (100 nm) were thermally evaporated in a vacuum chamber at  $\approx 6 \times 10^{-7}$  mbar, through a shadow mask. On each substrate, the intersection of the ITO pattern with the evaporated top contact formed two squares of 9 mm<sup>2</sup> area and two squares of 16 mm<sup>2</sup> area. The thickness of each layer was measured using a Veeco Dektak profilometer. The fabrication of the various device stacks including the photoactive and interlayers is further detailed in the Supporting Information.

**Characterization:** Both the measurement of the *J*-*V* curve and the EQE were performed under nitrogen atmosphere. Devices with MoO<sub>3</sub> were treated under a UV-lamp before the measurements. For these devices we found that this UV treatment gives more reproducible and occasionally better device performance. For the conventional tandem device we found a UV-treatment to be beneficial for the FF (+3%). Probably a similar photo-doping mechanism can occur for tin oxide as well, although we did not investigate the mechanism. The *J*-*V* characteristics were measured with a Keithley 2400 source meter from -2 to +2V (inverted cells) or +2 to -2V (conventional cells). Four hundred and one points per scan were acquired, each with 20 ms integration time. The lamp used for this measurement was a tungsten-halogen lamp which was filtered with a UV filter and a daylight filter (Hoya LB120). The color and intensity of the light were tuned in a way to match the EQE-integrated *J*<sub>SC</sub> of representative single-junction cells of the two subcells at the same time. The measurements were performed through an illumination mask with aperture sizes of 6.76 and 12.96 mm<sup>2</sup>, corresponding to the 9 and 16 mm<sup>2</sup> nominal device areas, respectively. This defined the active area of the devices.

The EQE measurement was performed in a home-made setup, consisting of a tungsten-halogen lamp, a chopper, a monochromator (Oriel, Cornerstone 130), a pre-amplifier (Stanford Research Systems SR570) and a lock-in amplifier (Stanford Research Systems SR830 DSP). The substrates were kept in a N<sub>2</sub>-filled box with a quartz window during the duration of the measurement. The device of interest on each substrate was aligned through a circular aperture with 2 mm of diameter, defining the active area. The signal response to the modulated light was transformed into an EQE value by comparison with the measurement on a calibrated silicon reference solar cell. The average standard deviation in measuring the wavelength-dependent EQE in this setup is less than 0.005 electrons/photons for wavelengths in the range of 350–1050 nm. The 530 and 940 nm bias lights were high power light-emitting diodes obtained from Thorlabs. The additional voltage bias was applied directly from the pre-amplifier. The voltage bias correction needed for the EQE of the tandems cells was approximated as the  $V_{OC}$  of the reference single-junction cells: 0.92 and 0.61 V for biasing the front and back subcells, respectively.

**Optical-Electrical Modeling:** Optical simulations based on the transfer matrix method was performed using Setfos 3.2 (Fluxim). The wavelength dependent *n* and *k* values of each active layer were determined by transmission and reflection measurements using an integrating sphere



attachment on a Perkin-Elmer Lambda 1050 spectrophotometer. The optimization based on IQE correction of the modeled current densities and the construction of the  $J$ - $V$  characteristics was performed according to a procedure previously reported.<sup>[48]</sup> According to the results discussed in Section 2.1, the performance of J71:ITIC in the conventional and inverted structure is more or less comparable. Therefore, the data series of the representative conventional cell of J71:ITIC was approximated with the dataset of the inverted representative cell, reported in Table S2, Supporting Information. The performance of the PMDPP3T:PC<sub>60</sub>BM series in the inverted configuration was taken from one of our previous work, where we utilized zinc oxide instead of tin oxide (Table S3, Supporting Information).<sup>[53]</sup> We then calculated the spectrally resolved fraction of absorbed photons from the subcells and we scaled this by the corresponding IQE (reported in Table S1–S3, Supporting Information). The result can be considered as an estimated EQE spectrum of the subcells. Integration with the reference AM1.5G solar spectrum follows to derive the  $J_{SC}$  of the subcells. At last, the construction of the  $J$ - $V$  characteristic of the tandem was performed as described in the referenced article.<sup>[48]</sup>

**Scanning Electron Microscopy:** For the SEM cross-section studies, layers on Si substrates were investigated using a Philips XL30S FEG microscope with a field emission cathode.

**Kelvin Probe:** The measurements of the surface potential were done with a McAllister KP6500 Kelvin-Probe (KP) system in vacuum ( $10^{-6}$  mbar). Highly ordered pyrolytic graphite with a work function of 4.5 eV was used as reference.

## Supporting Information

Supporting Information is available from the Wiley Online Library or from the author.

## Acknowledgments

We thank Dr. Harm van Eersel of Simbeyond B.V. for developing the software for the optical-electrical modeling and Tobias Haeger for his help with the SEM measurements. The research has received funding from the European Community's Seventh Framework Programme (FP7/2007-2013) (Grant Agreement no. 607585, project OSNIRO), the European Research Council (ERC Grant Agreement No. 339031), and the Ministry of Education, Culture, and Science (Gravity program 024.001.035).

## Conflict of Interest

The authors declare no conflict of interest.

## Keywords

tandem cell, tin oxide, polymer solar cells, conjugated polymers, fullerenes

Received: December 13, 2018

Revised: January 8, 2019

Published online: February 1, 2019

- [1] M. Kaltenbrunner, M. S. White, E. D. Glowacki, T. Sekitani, T. Someya, N. S. Sariciftci, S. Bauer, *Nat. Commun.* **2012**, *3*, 1772.  
[2] R. Ma, J. Feng, D. Yin, H.-B. Sun, *Org. Electron.* **2017**, *43*, 77.

- [3] Y. W. Li, G. Y. Xu, C. H. Cui, Y. F. Li, *Adv. Energy Mater.* **2018**, *8*, 1701791.  
[4] K.-S. Chen, J.-F. Salinas, H.-L. Yip, L. Huo, J. Hou, A. K.-Y. Jen, *Energy Environ. Sci.* **2012**, *5*, 9551.  
[5] C.-C. Chen, L. Dou, J. Gao, W. H. Chang, G. Li, Y. Yang, *Energy Environ. Sci.* **2013**, *6*, 2714.  
[6] G. Xu, L. Shen, C. Cui, S. Wen, R. Xue, W. Chen, H. Chen, J. Zhang, H. Li, Y. Li, Y. Li, *Adv. Funct. Mater.* **2017**, *27*, 1605908.  
[7] G. Li, R. Zhu, Y. Yang, *Nat. Photonics* **2012**, *6*, 153.  
[8] S. Zhang, Y. Qin, J. Zhu, J. Hou, *Adv. Mater.* **2018**, *30*, 1800868.  
[9] S. Li, L. Ye, W. Zhao, H. Yan, B. Yang, D. Liu, W. Li, H. Ade, J. Hou, *J. Am. Chem. Soc.* **2018**, *140*, 7159.  
[10] Z. Zheng, Q. Hu, S. Zhang, D. Zhang, J. Wang, S. Xie, R. Wang, Y. Qin, W. Li, L. Hong, N. Liang, F. Liu, Y. Zhang, Z. Wei, Z. Tang, T. P. Russell, J. Hou, H. Zhou, *Adv. Mater.* **2018**, *30*, 1801801.  
[11] R. Søndergaard, M. Hösel, D. Angmo, T. T. Larsen-Olsen, F. Krebs, *Mater. Today* **2012**, *15*, 36.  
[12] A. Furlan, R. A. J. Janssen, *Polymer Photovoltaics: Materials, Physics, and Device Engineering* (Eds: F. Huang, H.-L. Yip, Y. Cao), Royal Society of Chemistry, Cambridge **2016**, Chapter 11, pp. 310–351.  
[13] G. Li, W. H. Chang, Y. Yang, *Nat. Rev. Mater.* **2017**, *2*, 17043.  
[14] D. Di Carlo Rasi, R. A. J. Janssen, *Adv. Mater.* **2019**, *31*, 1806499.  
[15] Y. Cui, H. Yao, B. Gao, Y. Qin, S. Zhang, B. Yang, C. He, B. Xu, J. Hou, *J. Am. Chem. Soc.* **2017**, *139*, 7302.  
[16] Y. Qin, Y. Chen, Y. Cui, S. Zhang, H. Yao, J. Huang, W. Li, Z. Zheng, J. Hou, *Adv. Mater.* **2017**, *29*, 1606340.  
[17] L. Meng, Y. Zhang, X. Wan, C. Li, X. Zhang, Y. Wang, X. Ke, Z. Xiao, L. Ding, R. Xia, H.-L. Yip, Y. Cao, Y. Chen, *Science* **2018**, *361*, 1094.  
[18] J. Yang, R. Zhu, Z. Hong, Y. He, A. Kumar, Y. Li, Y. Yang, *Adv. Mater.* **2011**, *23*, 3465.  
[19] D. Di Carlo Rasi, K. H. Hendriks, G. H. L. Heintges, G. Simone, G. H. Gelinck, V. S. Gevaerts, R. Andriessen, G. Pirotte, W. Maes, W. Li, M. M. Wienk, R. A. J. Janssen, *Sol. RRL* **2018**, *2*, 1800018.  
[20] J. Gilot, M. M. Wienk, R. A. J. Janssen, *Appl. Phys. Lett.* **2007**, *90*, 143512.  
[21] J. Gilot, *PhD thesis*, Eindhoven University of Technology, Eindhoven **2010**, ISBN: 978-90-386-2279-8.  
[22] D. J. D. Moet, P. de Bruyn, P. W. M. Blom, *Appl. Phys. Lett.* **2010**, *96*, 153504.  
[23] S. Esiner, H. Van Eersel, M. M. Wienk, R. A. J. Janssen, *Adv. Mater.* **2013**, *25*, 2932.  
[24] W. Li, A. Furlan, K. H. Hendriks, M. M. Wienk, R. A. J. Janssen, *J. Am. Chem. Soc.* **2013**, *135*, 5529.  
[25] S. Lu, H. Lin, S. Zhang, J. Hou, W. C. H. Choy, *Adv. Energy Mater.* **2017**, *7*, 1701164.  
[26] S. Esiner, G. W. P. van Pruissen, M. M. Wienk, R. A. J. Janssen, *J. Mater. Chem. A* **2016**, *4*, 5107.  
[27] Y. Zhou, C. Fuentes-Hernandez, J. W. Shim, T. M. Khan, B. Kippelen, *Energy Environ. Sci.* **2012**, *5*, 9827.  
[28] J. Y. Kim, K. Lee, N. E. Coates, D. Moses, T.-Q. Nguyen, M. Dante, A. J. Heeger, *Science* **2007**, *317*, 222.  
[29] W.-S. Chung, H. Lee, W. Lee, M. J. Ko, N.-G. Park, B.-K. Ju, K. Kim, *Org. Electron.* **2010**, *11*, 521.  
[30] C.-C. Chen, L. Dou, J. Gao, W.-H. Chang, G. Li, Y. Yang, *Energy Environ. Sci.* **2013**, *6*, 2714.  
[31] K. Zhang, K. Gao, R. Xia, Z. Wu, C. Sun, J. Cao, L. Qian, W. Li, S. Liu, F. Huang, X. Peng, L. Ding, H.-L. Yip, Y. Cao, *Adv. Mater.* **2016**, *28*, 4817.  
[32] K. Zhang, B. Fan, R. Xia, X. Liu, Z. Hu, H. Gu, S. Liu, H.-L. Yip, L. Ying, F. Huang, Y. Cao, *Adv. Energy Mater.* **2018**, *8*, 1703180.  
[33] K. Zhang, R. Xia, B. Fan, X. Liu, Z. Wang, S. Dong, H.-L. Yip, L. Ying, F. Huang, Y. Cao, *Adv. Mater.* **2018**, *30*, 1803166.  
[34] H. Zhou, Y. Zhang, C.-K. Mai, S. D. Collins, G. C. Bazan, T.-Q. Nguyen, A. J. Heeger, *Adv. Mater.* **2015**, *27*, 1767.

- [35] Y. Cui, H. Yao, B. Gao, Y. Qin, S. Zhang, B. Yang, C. He, B. Xu, J. Hou, *J. Am. Chem. Soc.* **2017**, *139*, 7302.
- [36] J. Lee, H. Kang, S. Kee, S. H. Lee, S. Y. Jeong, G. Kim, J. Kim, S. Hong, H. Back, K. Lee, *ACS Appl. Mater. Interfaces* **2016**, *8*, 6144.
- [37] Y. Qin, Y. Chen, Y. Cui, S. Zhang, H. Yao, J. Huang, W. Li, Z. Zheng, J. Hou, *Adv. Mater.* **2017**, *29*, 1606340.
- [38] Y. Cui, H. Yao, C. Yang, S. Zhang, J. Hou, *Acta Polym. Sin.* **2018**, *2*, 223.
- [39] X. Che, Y. Li, Y. Qu, S. R. Forrest, *Nat. Energy* **2018**, *3*, 422.
- [40] Y. Gao, V. M. Le Corre, A. Gaïtis, M. Neophytou, M. A. Hamid, K. Takanabe, P. M. Beaujuge, *Adv. Mater.* **2016**, *28*, 3366.
- [41] Y. Ma, S.-C. Chen, Z. Wang, W. Ma, J. Wang, Z. Yin, C. Tang, D. Cai, Q. Zheng, *Nano Energy* **2017**, *33*, 313.
- [42] Q. Jiang, L. Zhang, H. Wang, X. Yang, J. Meng, H. Liu, Z. Yin, J. Wu, X. Zhang, J. You, *Nat. Energy* **2016**, *2*, 16677.
- [43] S. Trost, K. Zilberberg, A. Behrendt, T. Riedl, *J. Mater. Chem.* **2012**, *22*, 16224.
- [44] S. Trost, T. Becker, A. Polywka, P. Görrn, M. F. Oszejca, N. A. Luechinger, D. Rogalla, M. Weidner, P. Reckers, T. Mayer, T. Riedl, *Adv. Energy Mater.* **2016**, *6*, 1600347.
- [45] T. Becker, S. Trost, A. Behrendt, I. Shutsko, A. Polywka, P. Görrn, P. Reckers, C. Das, T. Mayer, D. Di Carlo Rasi, K. H. Hendriks, M. M. Wienk, R. A. J. Janssen, T. Riedl, *Adv. Energy Mater.* **2018**, *8*, 1702533.
- [46] Z.-G. Zhang, B. Qi, Z. Jin, D. Chi, Z. Qi, Y. Li, J. Wang, *Energy Environ. Sci.* **2014**, *7*, 1966.
- [47] H. Bin, L. Gao, Z. G. Zhang, Y. Yang, Y. Zhang, C. Zhang, S. Chen, L. Xue, C. Yang, M. Xiao, Y. Li, *Nat. Commun.* **2016**, *7*, 13651.
- [48] J. Gilot, M. M. Wienk, R. A. J. Janssen, *Adv. Mater.* **2010**, *22*, E67.
- [49] J. Gilot, M. M. Wienk, R. A. J. Janssen, *Adv. Funct. Mater.* **2010**, *20*, 3904.
- [50] R. Timmreck, T. Meyer, J. Gilot, H. Seifert, T. Mueller, A. Furlan, M. M. Wienk, D. Wynands, J. Hohl-Ebinger, W. Warta, R. A. J. Janssen, M. Riede, K. Leo, *Nat. Photonics* **2015**, *9*, 478.
- [51] K. H. Hendriks, G. H. L. Heintges, V. S. Gevaerts, M. M. Wienk, R. A. J. Janssen, *Angew. Chem. Int. Ed.* **2013**, *52*, 8341.
- [52] Y. Sun, J. H. Seo, C. J. Takacs, J. Seifert, A. J. Heeger, *Adv. Mater.* **2011**, *23*, 1679.
- [53] D. Di Carlo Rasi, K. H. Hendriks, M. M. Wienk, R. A. J. Janssen, *Adv. Energy Mater.* **2017**, *7*, 1701664.